The Climatological Distribution of Potential Vorticity over the Abyssal Ocean

JANE O'DWYER AND RICHARD G. WILLIAMS

Oceanography Laboratories, Department of Earth Sciences, University of Liverpool, Liverpool, United Kingdom

(Manuscript received 22 January 1996, in final form 25 April 1997)

ABSTRACT

Climatological maps of the large-scale potential vorticity field Q along isopycnals are diagnosed for the abyssal waters over the global ocean. The inferred patterns of Q vary with density, the basin, and hemisphere. At middepths, the distribution of Q is controlled by the background planetary vorticity gradient. On deeper isopycnals, there are regions where Q contours deviate from latitude circles and even regions of nearly uniform Q. These different regimes appear to be robust features over the interior of ocean basins, as the standard error is found to be relatively small there. The nearly uniform Q occurs in the deep waters of the North Pacific and, possibly, in the bottom waters of the western North Atlantic and North Pacific. The nearly uniform Q has a low magnitude in each case, as well as a relatively low variability for the deep waters of the North Pacific. This nearly uniform Q signal appears to be formed when a single water mass enters the basin from a low latitude source.

1. Introduction

The theoretical focus in understanding the circulation of the upper ocean has been on the large-scale potential vorticity Q:

$$Q = -\frac{f}{\overline{\rho}}\frac{\partial \sigma}{\partial z}. \tag{1}$$

Here f is planetary vorticity, σ is potential density, z is the vertical coordinate, and $\overline{\rho}$ is a reference density. Climatological maps of Q over the upper kilometer show how the gyre circulation can be separated into regions of open, closed, and blocked Q contours (McDowell et al. 1982; Keffer 1985) (Fig. 1). These different regimes have been associated with different paradigms of the circulation involving (i) ventilation along open Q contours (Luyten et al. 1983) or (ii) eddy homogenization within closed Q contours (Rhines and Young 1982a), although these differences become obscured if ventilation forms nearly uniform Q (Williams 1991). In addition, Talley and McCartney (1982) employ Q as a dynamical tracer to infer the circulation of Labrador Sea Water.

In contrast, there has been less discussion of the Q field in the observations or theoretical models of the deep ocean. Stommel and Arons (1960) provided the first theoretical picture of the deep circulation consisting of a poleward interior flow supplied by deep western boundary currents; see the review by Warren (1981). However, this linearized model implies a particularly restrictive Q distribution in the ocean interior that may not be relevant to the real ocean (see section 2).

Consider the potential vorticity variations for a single layer of fluid with thickness h. Then Q in (1) can be interpreted as

$$Q = \frac{f}{h}, \tag{2}$$

and its rate of change following a fluid parcel is given by

$$\frac{DQ}{Dt} = \mathcal{F} - \mathcal{D}, \tag{3}$$

where $\mathcal{F}$ and $\mathcal{D}$ represent forcing and dissipation of Q, $D/Dt = \partial/\partial t + \mathbf{u}\cdot\nabla$ is the substantial derivative, and $\mathbf{u}$ is the horizontal velocity vector. Thus, fluid parcels only change their Q through the action of forcing or dissipation. In the steady state, expanding the substantial derivative in (3) gives

$$\frac{DQ}{Dt} = \frac{\beta v}{h} - \frac{f}{h^2}\mathbf{u}\cdot\nabla h, \tag{4}$$

where v is the northward velocity and $\beta = df/dy$. Here we choose to define linear and nonlinear Q regimes according to the relative importance of the planetary vorticity and thickness terms on the right-hand side of (4). Taking the ratio of these advective terms in (4) gives

$$-\frac{f}{h^2}\mathbf{u}\cdot\nabla h \Big/ \frac{\beta v}{h} \sim \frac{\Delta h}{h} \Big/ \frac{\Delta f}{f}. \tag{5}$$

Corresponding author address: Dr. Richard G. Williams, Oceanography Laboratories, Department of Earth Sciences, The University of Liverpool, Bedford Street North, P.O. Box 147, Liverpool L69 3BX, United Kingdom.
E-mail: ric@liv.ac.uk

© 1997 American Meteorological Society

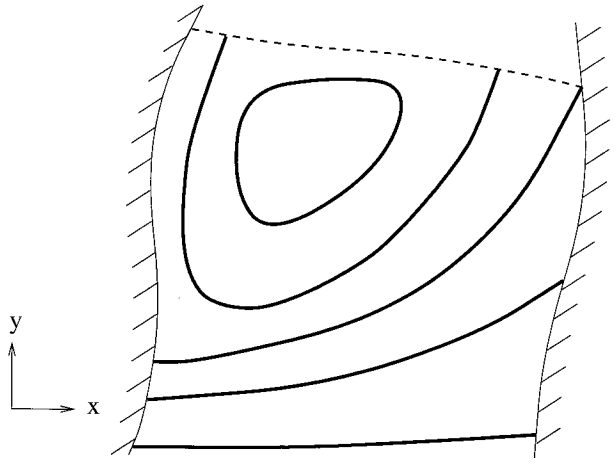

FIG. 1. Schematic plan view of the large-scale potential vorticity Q on an isopycnal in the upper ocean. The Q contours (full lines) are either (i) open—threading to and from the outcrop (dashed line), (ii) closed—possibly enclosing uniform Q, or (iii) blocked—running from coast to coast.

The linear regime is defined by $|(\Delta h/h)/(\Delta f/f)| \ll 1$, where changes in Q are controlled by changes in planetary vorticity. In this case, Q contours follow latitude circles and any meridional flow must be forced in order for fluid parcels to cross Q contours.

The nonlinear regime is defined by $|(\Delta h/h)/(\Delta f/f)| \sim 1$, where thickness variations are comparable to those of planetary vorticity. In this case, Q contours are inclined to latitude circles and Q may even become homogeneous.

Typical values for the Antarctic Bottom Water (AABW) in the western North Atlantic of $f \sim 10^{-4}$ s^{-1}, $\Delta f \sim 5 \times 10^{-5}$ s^{-1}, $h \sim 1000$ m, and $\Delta h \sim 500$ m suggest that $|(\Delta f/f)/(\Delta h/h)| \sim 1$, implying that Q contours depart from latitude circles. Consequently, we diagnose Q from climatology to see whether linear or nonlinear regimes exist in the abyssal ocean.

In section 2, the Q distribution is discussed further for the idealized deep circulation models of Stommel and Arons (1960) and Speer and McCartney (1992). In section 3, the method is described for calculating Q from bottle data within the National Oceanographic Data Center (NODC) climatology. In section 4, the inferred Q distributions are shown, firstly, along a meridional section through the Pacific and, secondly, along σ surfaces intersecting the deep and bottom waters over the globe. The robustness of these Q maps is revealed by including maps of the standard error. Finally, in section 5, the implications of these diagnosed Q distributions are discussed.

2. Potential vorticity in idealized, deep circulation models

Consider the following idealized models of the deep circulation in terms of the implied Q distribution. In the Stommel–Arons model, an upwelling of cold water leads to a poleward interior flow (Fig. 2a), from the linear vorticity balance;

$$\beta v = f\frac{\partial w}{\partial z}, \tag{6}$$

where w is the vertical velocity. If the thickness of the layer is assumed to be constant, Q follows latitude circles, with the ratio $(\Delta h/h)/(\Delta f/f) \equiv 0$. Streamlines cross the zonal background Q contours (Fig. 2b) forced by the implicit diffusive heating in the model needed to balance the upwelling of cold water.

Speer and McCartney (1992) extend the Stommel–Arons model by allowing the layer thickness to vary so as to examine the spreading and grounding of AABW in the western North Atlantic (Fig. 2c). While there is the same imposed upwelling velocity and linear vorticity balance (6), the resulting poleward flow now induces $O(1)$ variations in layer thickness. Contours of the implied Q field now have a significant north–south component and in some regions are closely aligned with streamlines (Fig. 2d).

In contrast, Rhines and Young (1982a) argue that stirring by geostrophic eddies tends to homogenize Q within closed, time-mean, geostrophic streamlines. This end state of uniform Q leads to the possibility of free, recirculating flow, as fluid parcels have no background Q contours to cross. This hypothesis has been principally advocated for the main thermocline in the quasigeostrophic limit (Rhines and Young 1982b). If there is uniform Q over the large-scale in the deep waters, then there is automatically a more nonlinear balance in (4) with $|(\Delta h/h)/(\Delta f/f)| \sim 1$.

Following our scale analysis of the above models, we now diagnose Q from climatological data to see whether there are linear or nonlinear regimes in the abyssal waters.

3. Analysis of climatological data

a. Calculating properties along potential density surfaces

The data used in this analysis is observed level bottle data held as of 1993 by NODC; see Levitus and Boyer (1994a, b) and Levitus et al. (1994) for descriptions of the temperature, oxygen, and salinity data. Following Lozier et al. (1994), we perform our data analysis on isopycnal surfaces, as isobaric smoothing artificially distorts water mass properties. The following algorithm is applied:

1) For each station, potential density σ_n is calculated at every observed level from in situ temperature and salinity. The potential density is calculated relative to an appropriate reference pressure; the subscript n refers to this reference pressure in 1000 decibars.
2) The depth, $z(\sigma_n)$, of the σ_n surface at each station is

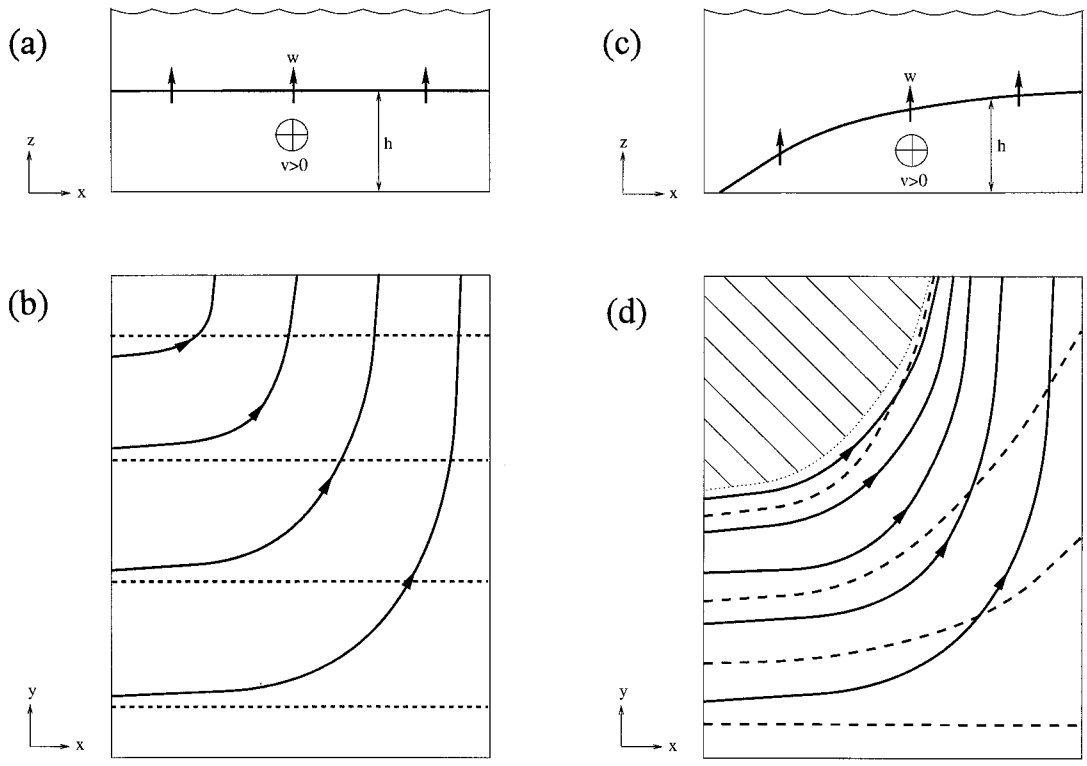

FIG. 2. Schematic figure showing (a) a zonal section and (b) a plan view for the Stommel and Arons (1960) model, and likewise (c) and (d) for the Speer and McCartney (1992) model. The models differ in the layer thickness h being assumed constant in Stommel and Arons, but allowed to vary in Speer and McCartney. The resulting Q contours (dashed lines) follow latitude circles in (b) but are strongly inclined to latitude circles in (d). In both cases, the forcing drives streamlines (full lines) across the Q contours. The hatched region in (d) represents where the layer has grounded.

determined by linear interpolation between the bounding observed levels.

3) Q is evaluated along σ_n from the planetary vorticity and the vertical spacing of σ_n surfaces using the finite difference form of (1) (Fig. 3),

$$Q = -\frac{f}{(1000 + \sigma_n)} \frac{\Delta\sigma_n}{[z(\sigma_n + \Delta\sigma_n/2) - z(\sigma_n - \Delta\sigma_n/2)]},$$

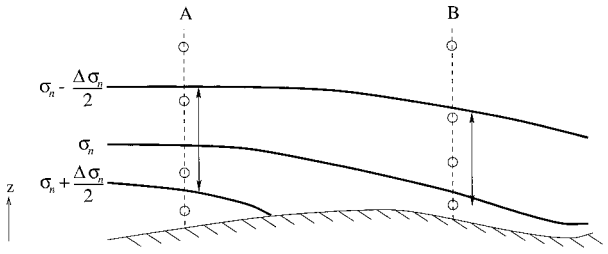

FIG. 3. Cross section showing the calculation of Q at two stations, A and B, indicated by vertical dashed lines. Observed levels are denoted by open circles and isopycnals by full lines. At station A, Q is evaluated on σ_n from the density gradient between the isopycnals $\sigma_n - \Delta\sigma_n/2$ and $\sigma_n + \Delta\sigma_n/2$. At station B where the lower isopycnal has grounded, Q is evaluated on σ_n from the density gradient between the upper isopycnal, $\sigma_n - \Delta\sigma_n/2$, and the deepest observed level at a depth of $z(\sigma_{nb})$, where the density is σ_{nb}.

where $\Delta\sigma_n = 0.02$ is the density difference centered on σ_n. In regions where the denser bounding surface, $\sigma_n + \Delta\sigma_n/2$, does not exist due to grounding at the sea bed, then Q is calculated using the potential density σ_{nb} and depth $z(\sigma_{nb})$ of the deepest observed level:

$$Q = -\frac{f}{(1000 + \sigma_n)} \frac{\sigma_{nb} - (\sigma_n - \Delta\sigma_n/2)}{[z(\sigma_{nb}) - z(\sigma_n - \Delta\sigma_n/2)]}.$$

See the appendix for a comparison with the large-scale potential vorticity diagnosed from the vertical spacing of neutral surfaces, as advocated by McDougall (1988) and You and McDougall (1990).

b. Mapping the inferred property fields

In order to contour the data it is necessary to remove unrepresentative data points with extreme values. The following algorithm is applied:

1) Every basin is divided into 15° squares, and the mean and standard deviation of the isopycnal depth is calculated in each square.
2) Data points with the isopycnal depth outside three standard deviations of the mean for the square are discarded.

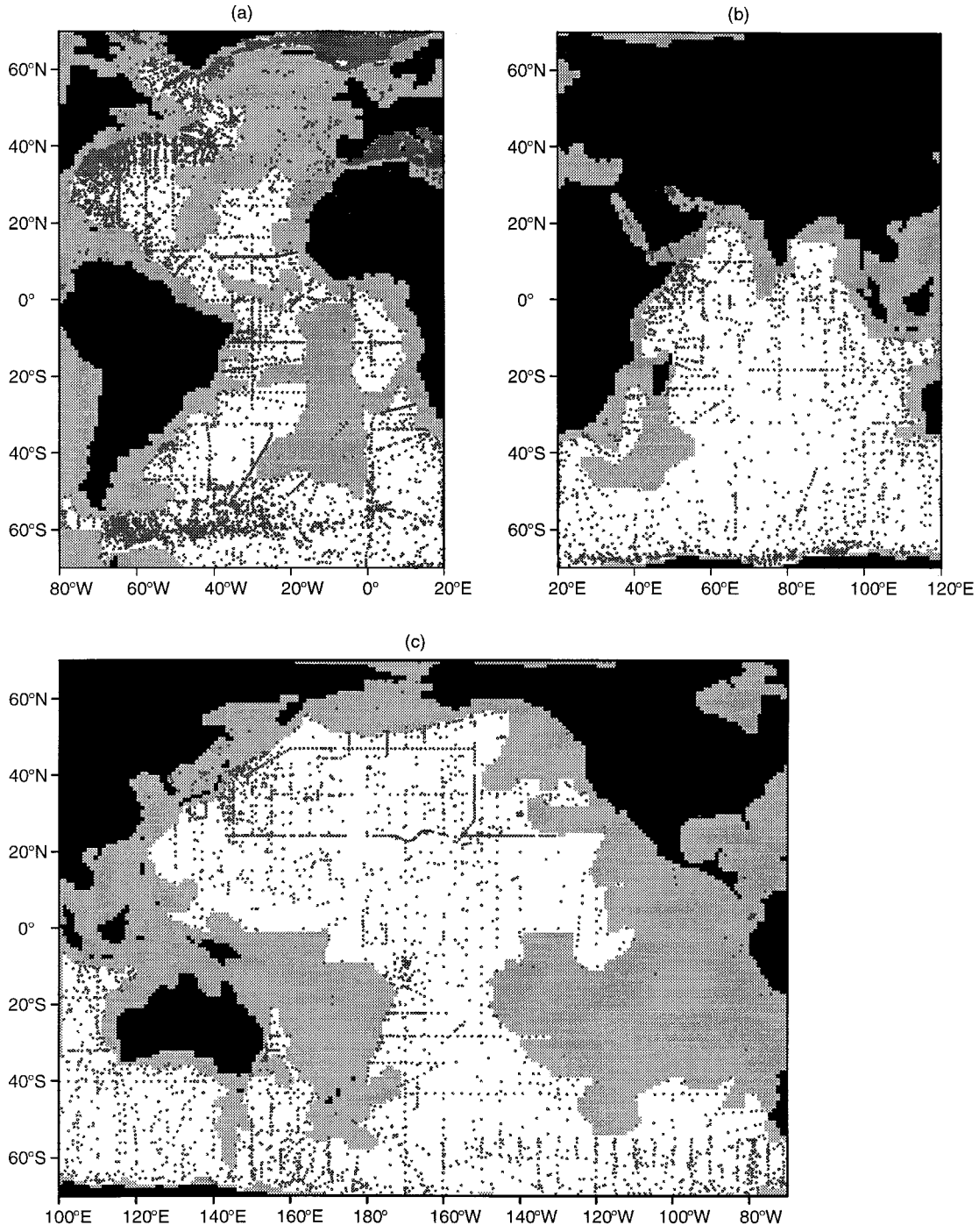

FIG. 4. The data points used in the diagnosis of Q on $\sigma_4 = 45.87$ in the deep interior basins for the (a) Atlantic, (b) Indian, and (c) Pacific Oceans. Data in shaded areas are excluded from the contouring of the fields; they include topography, data-poor regions, and shelf-sea basins.

3) Steps (1) and (2) are repeated once.
4) Any remaining spikes are removed subjectively by hand. In total, less than 3% of the data points within the deep water are removed from the surfaces examined. Figure 4 shows the data points retained along $\sigma_4 = 45.87$ over the globe.
5) Values of Q for data points in shallow water and near topography tend to have larger magnitudes than

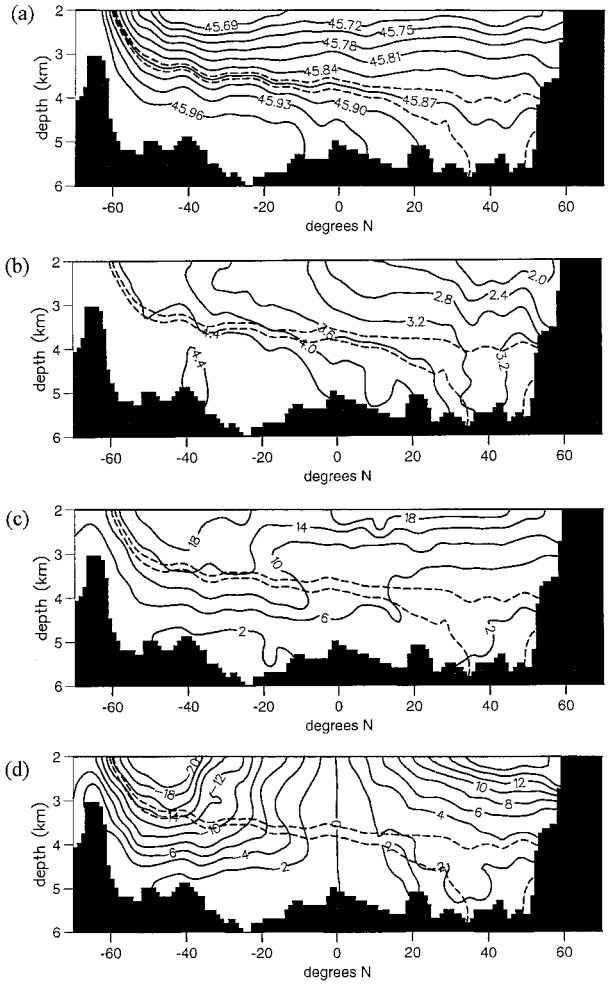

FIG. 5. Meridional section in the Pacific derived from station data between 160°W and 180°: (a) σ_4, (b) dissolved oxygen concentration (ml l^{-1}), (c) buoyancy frequency squared, $N^2 = -(g/\overline{\rho})\partial\sigma_4/\partial z$ ($10^{-7}s^{-2}$), and (d) large-scale potential vorticity, $Q = fN^2/g$ (10^{-12} m^{-1} s^{-1}). The positions of the isopycnals $\sigma_4 = 45.86$ and 45.88 are shown by the dashed lines.

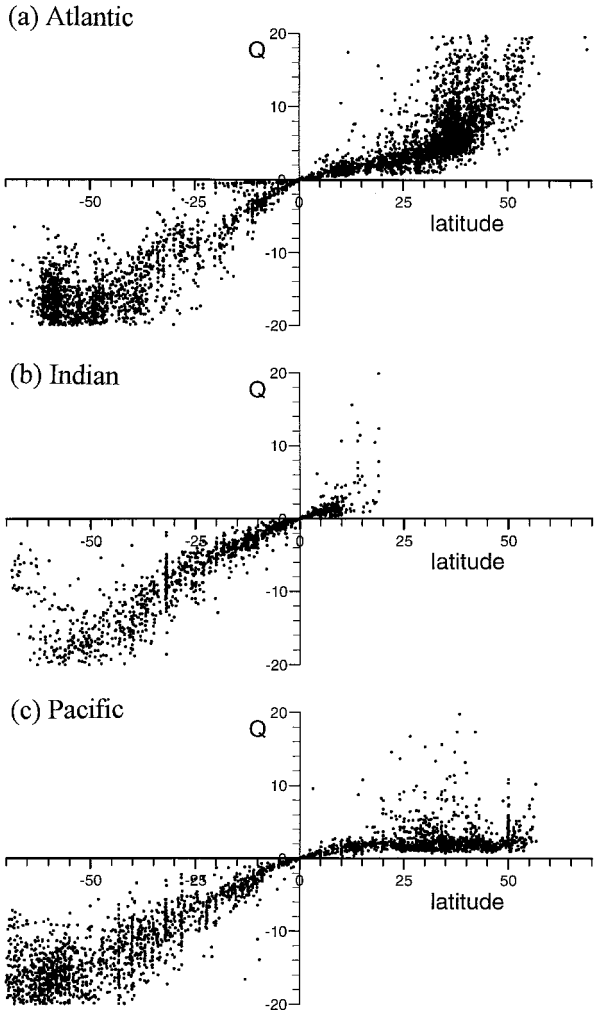

FIG. 6. Scatterplots showing Q (10^{-12} m^{-1} s^{-1}) variation with latitude on the $\sigma_4 = 45.87$ surface in the (a) Atlantic, (b) Indian, and (c) Pacific Oceans.

those in basin interiors and can become smeared out when the points are interpolated onto a regular grid, distorting the contouring of interior values. To prevent this happening, an ''interior region'' is defined over which the interpolation is performed (unshaded regions in Fig. 4).

6) The remaining interior data points are binned and interpolated onto a 1° grid and contoured.

4. Potential vorticity distributions

a. Meridional section in the Pacific

The Q distribution inferred from climatology is discussed, first, for a meridional section through the mid-Pacific and, second, along potential density surfaces intersecting deep and bottom water over the globe.

The variations of σ_4, dissolved oxygen concentration O_2, the square of buoyancy frequency N^2, and Q are shown in Fig. 5 for a meridional section through the mid-Pacific calculated from stations lying between 160°W and 180°. The σ_4 surfaces shoal between 45° and 70°S in the Antarctic Circumpolar Current (ACC) (Fig. 5a). Elsewhere, σ_4 surfaces lighter than 45.84 are relatively flat, whereas denser surfaces ground toward the north. These deep waters are ventilated from the Southern Ocean, as supported by the general decrease in O_2 to the north and middepths shown in Fig. 5b.

The stratification as measured by the buoyancy frequency N, where $N^2 = -(g/\overline{\rho})\partial\sigma_4/\partial z$, decreases with depth and toward the north for the deeper waters (Fig. 5c).

The variation in Q is related to changes in planetary vorticity and stratification $Q = fN^2/g$. First, the vari-

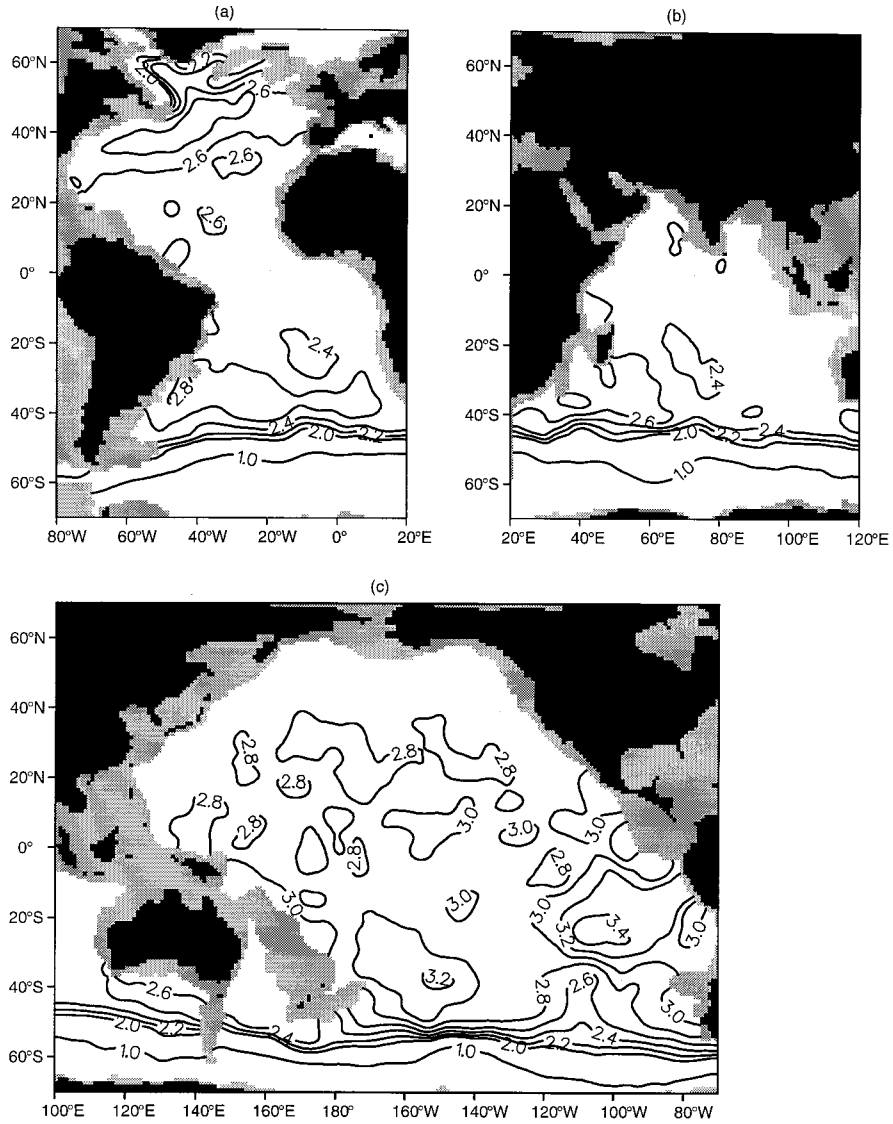

FIG. 7. Depth of $\sigma_3 = 41.44$ surface (km) in the (a) Atlantic, (b) Indian, and (c) Pacific Oceans.

ation in the planetary vorticity leads to negative values in the Southern Hemisphere, zero at the equator,[1] and positive values in the Northern Hemisphere. Second, the decrease in stratification with depth leads to lower magnitude Q in the deep waters. Thus, isopleths of Q fan out to the north and south from a minimum at the equator in the upper waters to low values extending over most of the denser waters (Fig. 5d).

The meridional gradients in Q along σ_4 surfaces are greatest over the upper waters, across the Tropics, and close to the ACC, as is evident by the relatively vertical isopleths of Q in Fig. 5d. The Tropics are marked by a large beta-controlled variation in Q extending from typically 25°S to 25°N (as discussed for the Atlantic by Suga and Talley 1995). Thus, the potential vorticity barrier to meridional flow across the equator is not the local change in sign of f across the equator, but rather the large meridional gradient in Q across the Tropics together with the zonal nature of Q as f approaches zero.

There are smaller meridional gradients in Q on σ_4 surfaces across the North Pacific than the South Pacific. This signal is consistent with the general northward decrease in N^2 for the deep waters of the Pacific. In terms of $Q = fN^2/g$, this N^2 variation opposes the poleward increase in f in the North Pacific, whereas

[1] Near the equator, as f approaches zero, the horizontal components of potential vorticity (and perhaps also the relative vorticity) become more important than the vertical component of potential vorticity. Thus, our analysis of the vertical component of potential vorticity is only useful away from the equator. Hua et al. (1997) argue that symmetric instability occurs along the equator making the full potential vorticity become zero.

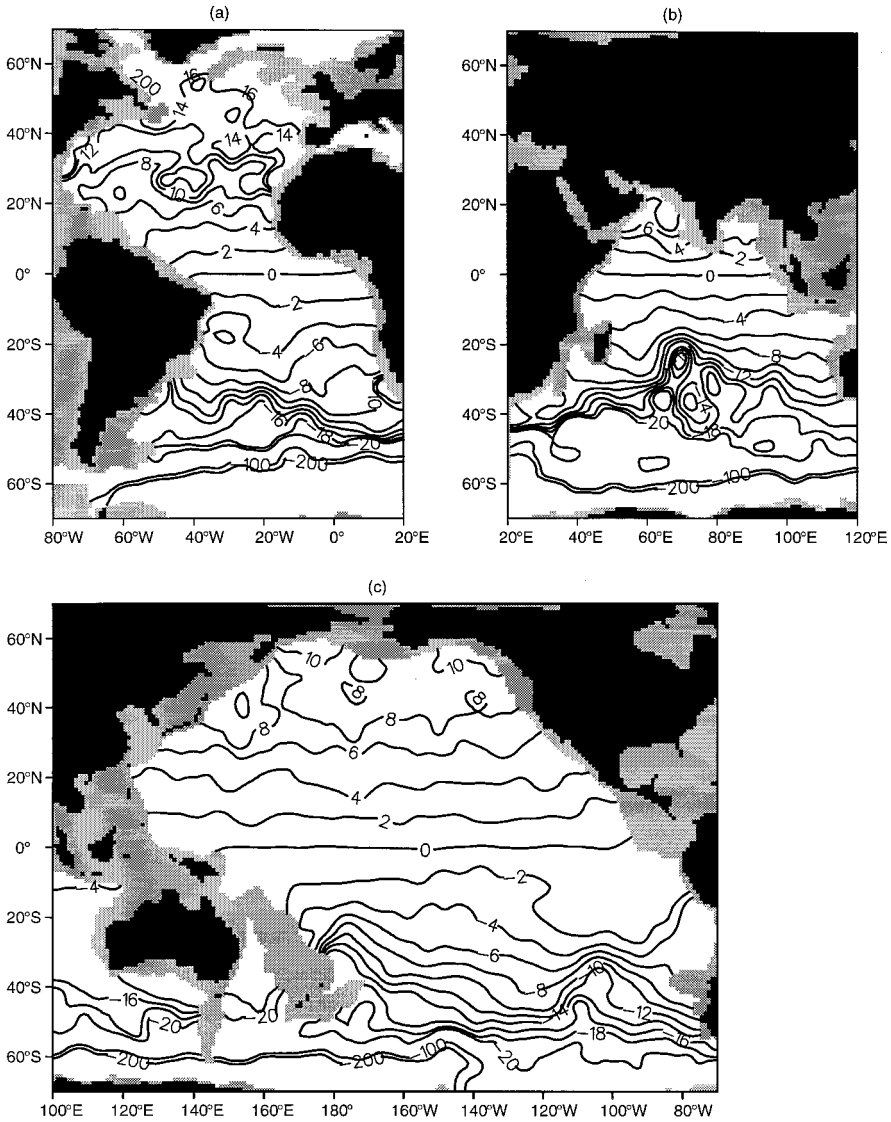

FIG. 8. Distribution of Q (10^{-12} m^{-1} s^{-1}) on $\sigma_3 = 41.44$ surface with $\Delta\sigma_3 = 0.02$ in the (a) Atlantic, (b) Indian, and (c) Pacific Oceans.

the N^2 and f variations reinforce each other over the South Pacific.

For example, consider the density layer defined by $\sigma_4 = 45.87 \pm 0.01$ shown by the dashed lines in Fig. 5. Here N^2 decreases from 14×10^{-7} s^{-2} at 40°S, to 8×10^{-7} s^{-2} at the equator, and decreases further to 2×10^{-7} s^{-2} by 40°N. Accordingly, there is a large change in Q from -14×10^{-12} m^{-1} s^{-1} at 40°S to zero at the equator, but a small change from the equator to 2×10^{-12} m^{-1} s^{-1} at 40°N. Interestingly, there also appear slightly larger changes in O_2 across the South Pacific than the North Pacific, with values of 4.4 ml l^{-1} at 40°S, 3.6 ml l^{-1} at the equator, and 3.2 ml l^{-1} at 40°N. These variations are investigated further in the next section by showing maps of Q, N^2, and O_2 along the $\sigma_4 = 45.87$ surface.

b. Isopycnal maps of potential vorticity

The variations of Q within the deep and bottom waters over the globe are now examined by focusing on the distributions along the $\sigma_3 = 41.44$, $\sigma_4 = 45.87$, and 45.90 surfaces, which range in depth from 2.5 to 5 km over the globe. We nominally refer to these surfaces as being for the upper deep water, deep water, and bottom water respectively, although the validity of these names depends on the water mass and basin.

These surfaces intersect the layers over which two of the most important water masses, NADW and AABW, spread over the globe (see the review by Schmitz 1995). NADW is formed from a mixture of northern overflow waters in the western North Atlantic (Dickson and

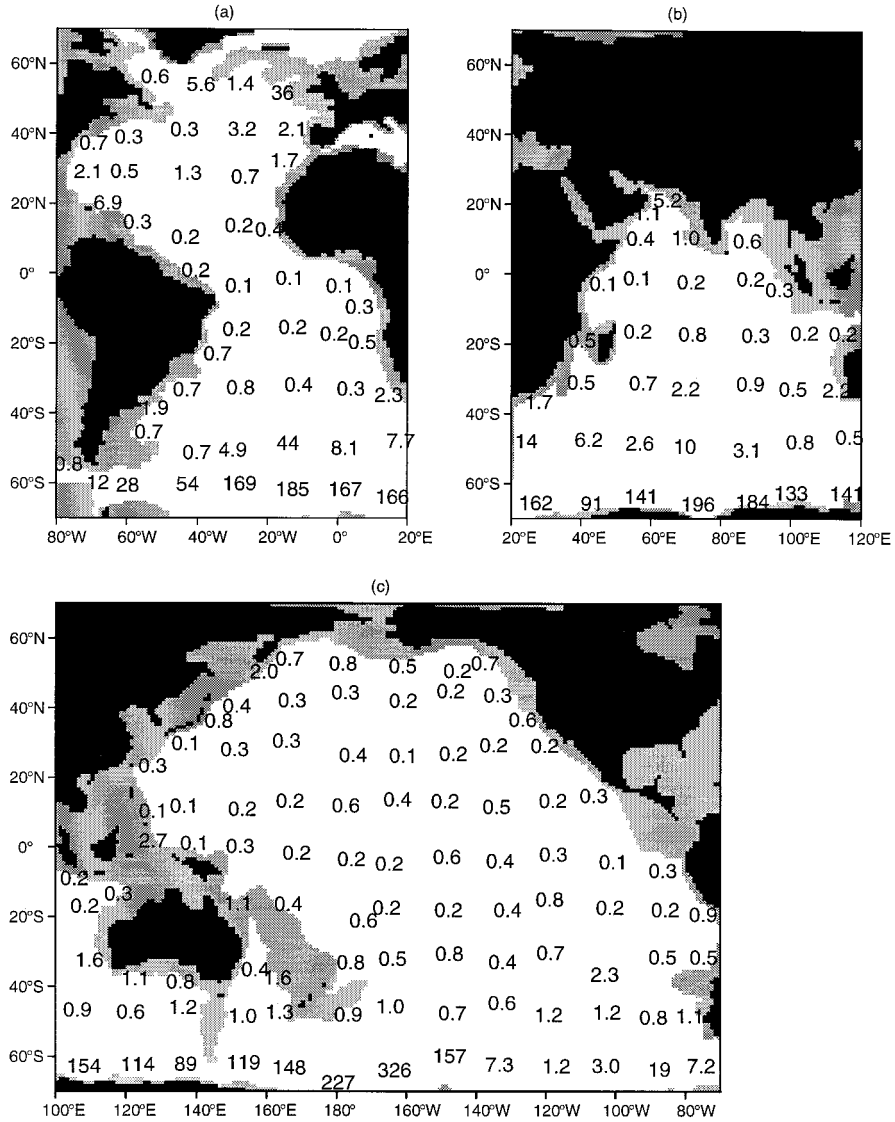

FIG. 9. Standard error in Q (10^{-12} m^{-1} s^{-1}) on $\sigma_3 = 41.44$ surface evaluated from data points within 15° squares in the (a) Atlantic, (b) Indian, and (c) Pacific Oceans.

Brown 1994). It flows southward in a deep western boundary current with recirculating components and eventually crosses the equator into the South Atlantic (McCartney 1993). NADW spreads into the eastern Atlantic through low latitude fracture zones in the Mid-Atlantic Ridge. The depth of NADW gradually increases from typically 2 to 4 km as it spreads over the Atlantic. In the ACC, NADW mixes with Circumpolar Water (CPW) and spreads into the Indian and Pacific Oceans (Reid and Lynn 1971). AABW is formed near Antarctica and spreads northward as the bottom water in all three ocean basins. As the water masses spread, their properties are modified through mixing, revealed by the northward warming of bottom water (Mantyla and Reid 1983).

It is difficult to define a unique characteristic σ surface for each water mass over the entire globe due to the modification of properties by mixing. Accepting this caveat, we nominally view our upper deep water as intersecting the layer over which NADW spreads over the western North Atlantic, deep water as the layer over which CPW and NADW spread over much of the globe, and bottom water as the layer over which AABW spreads.

To provide a context for the following isopycnal maps, we first show scatterplots of Q versus latitude for the deep water in the Atlantic, Indian, and Pacific basins (Fig. 6). The Q plots again reflect the control of f, with a zero value by definition at the equator, positive values to the north, and negative to the south. The basins generally have a similar scatter in the Southern Hemisphere with variability increasing southward to the ACC. How-

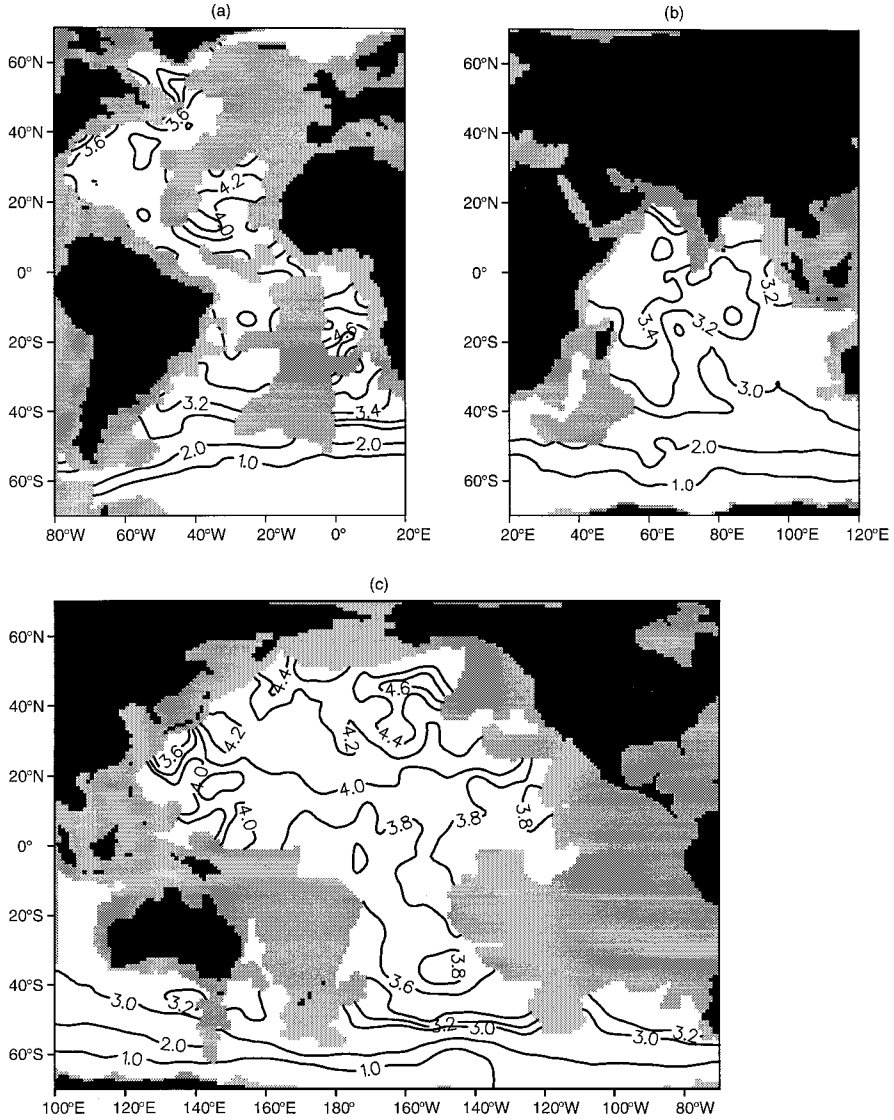

FIG. 10. As in Fig. 7 but for the depth of the $\sigma_4 = 45.87$ surface.

ever, there are differences in the Northern Hemisphere with a smaller scatter over the North Pacific than over the North Atlantic. This different scatter is probably due to there being a single water-mass source for the North Pacific compared with a range of sources in the North Atlantic.

Our focus is to highlight how the Q distribution varies for each of these surfaces over the globe. The robustness of each Q map is revealed by including estimates of the standard error calculated as follows: first, the standard deviation Q is evaluated from the range in data values contained within each of the 15° squares covering the domain; second, the standard error is estimated from $Q_{\text{std}}/n_i^{1/2}$, where n_i is the number of independent data points in each square. Data points are defined here to be independent if either they are from different years or are more than 1° apart.

1) UPPER DEEP WATER: $\sigma_3 = 41.44$ SURFACE

This σ_3 surface typically lies at a depth of 2.5 km in the Atlantic and Indian Oceans and deepens to 3 km in the Pacific (Fig. 7). The surface shoals markedly across the ACC in each of the oceans.

The inferred Q distribution appears to be broadly symmetric across the Northern and Southern Hemispheres with Q contours generally following latitude circles (Fig. 8). There is a large contrast in Q across the ACC in all the oceans, also revealed in the Pacific section (Fig. 5). The Q contours within the basins intersect the continental barriers and prevent any free meridional flow. There are some departures from the zonal configuration with Q contours slightly inclined from latitude circles in the South Atlantic and South Pacific. On a smaller scale, there are some closed-off high Q contours in the eastern and central North

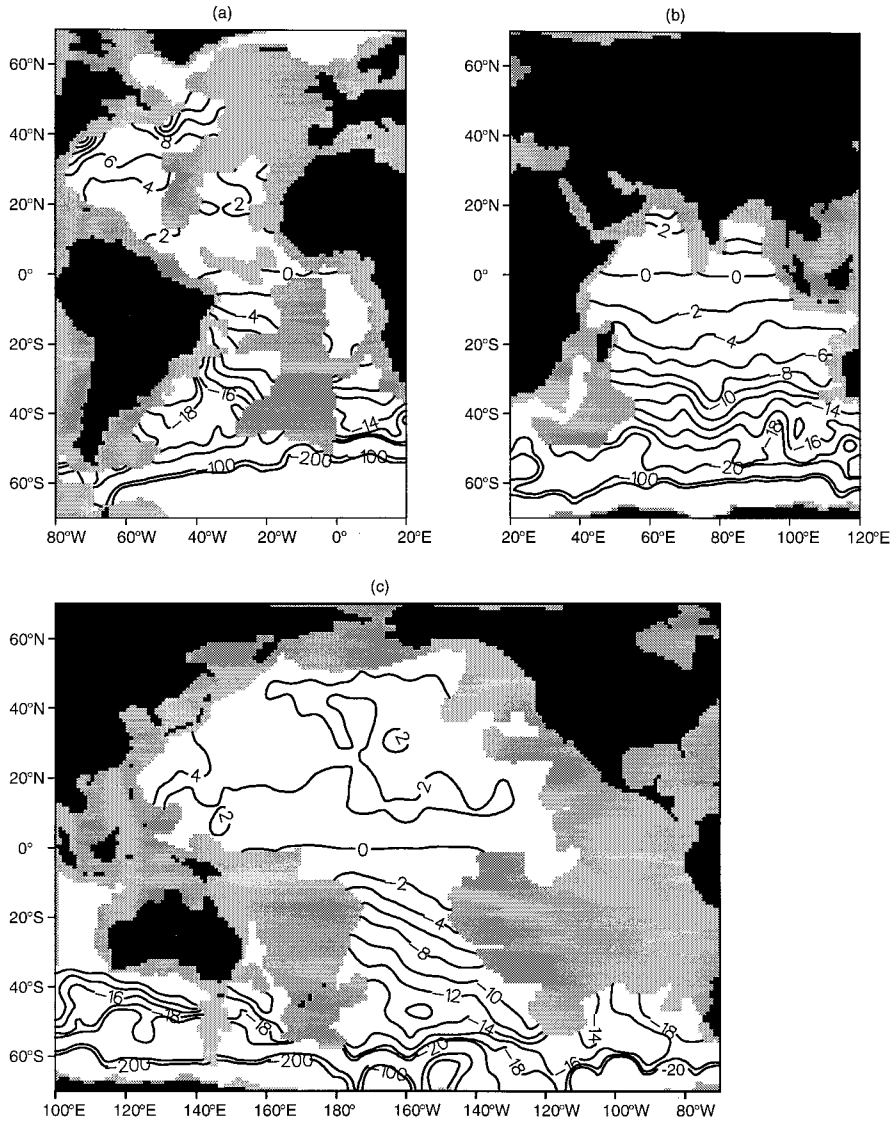

FIG. 11. As in Fig. 8 but for Q on the $\sigma_4 = 45.87$ surface with $\Delta\sigma_4 = 0.02$.

Atlantic and near the Kerguelan Plateau in the Indian Ocean; however, the standard error approaches 3×10^{-12} m^{-1} s^{-1} in these locations, which is a similar magnitude to these anomalies (Fig. 9).

2) DEEP WATER: $\sigma_4 = 45.87$ SURFACE

This σ_4 surface lies between 3.5 and 4 km in the Atlantic and Pacific Oceans and is slightly shallower, at a depth between 3 and 3.5 km, in the Indian Ocean (Fig. 10). Again, there is a marked shoaling across the ACC in all the oceans. At this depth, the Atlantic is separated into western and eastern basins by the Mid-Atlantic Ridge with the principal exchange occurring through fracture zones close to the equator. The Pacific Ocean is also more confined at these depths.

The inferred Q field for this deep water (Fig. 11) reveals a more complex structure than seen in the upper deep water, except for the Indian Ocean where the Q structure remains broadly zonal. In the western Atlantic, the magnitude of Q increases poleward in both hemispheres, but with a smaller meridional gradient over the Northern Hemisphere. While Q contours are generally blocked here, they are more inclined away from latitude circles than in the upper deep water. In the eastern Atlantic, there is a much reduced contrast in Q with some regions appearing to have nearly uniform Q.

The Q variation in the Pacific for the deep water is strikingly different to the upper deep water with a north–south asymmetry appearing. In the South Pacific, Q contours are strongly inclined to latitude circles, which presents a free path for meridional flow in the interior. The increase in the inclination of these contours with depth

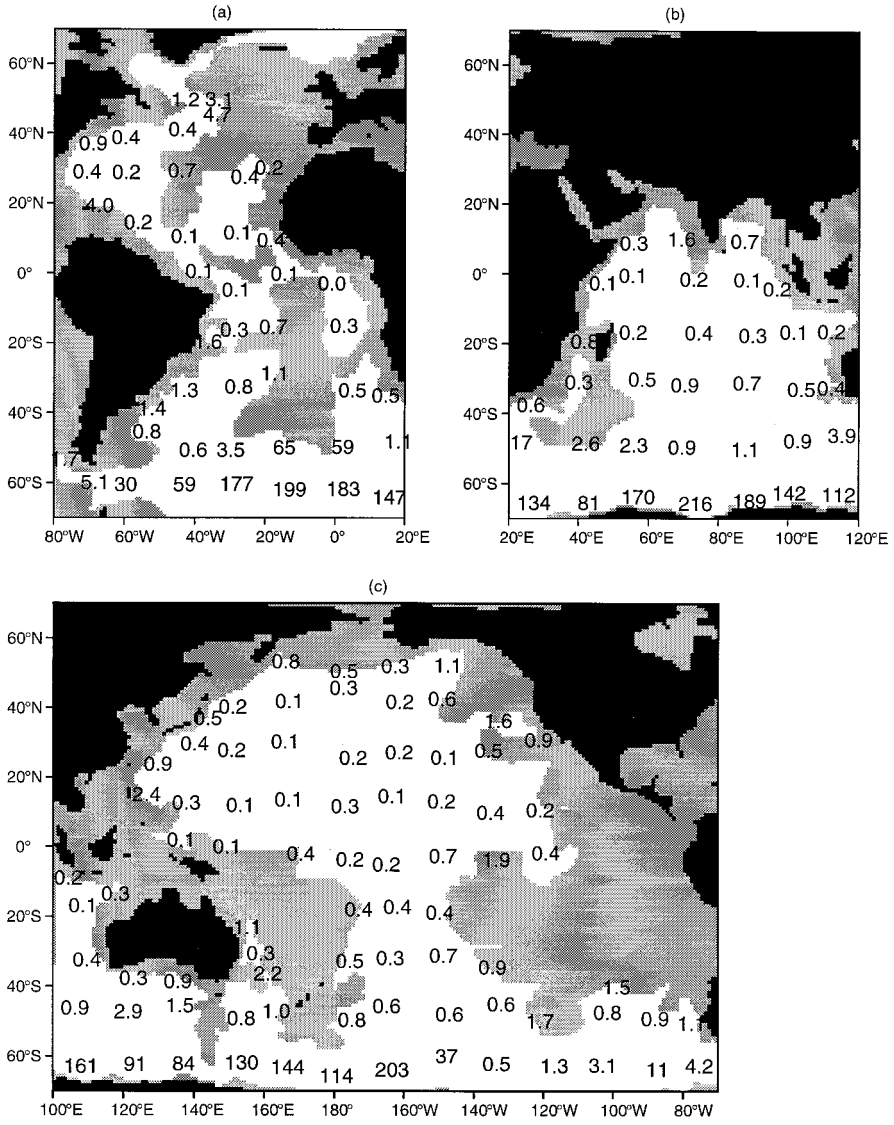

FIG. 12. As in Fig. 9 but for standard error on the $\sigma_4 = 45.87$ surface.

implies that the flow is more nonlinear here than in the overlying upper deep water.

In the North Pacific Q is relatively low in magnitude and nearly homogeneous with a value of 2×10^{-12} m^{-1} s^{-1}. Note that the scatter in Q is also relatively low in the North Pacific, as shown in Fig. 6. Along this σ surface, there may even be a recirculating free flow due to the nearly uniform Q, although the flow is still connected by thermal wind to the overlying σ surfaces where there are Q gradients.

These regions of nearly uniform Q appear to be relatively robust since the standard error is typically between 0.1 and 0.3×10^{-12} m^{-1} s^{-1} in the interior of the North Pacific and 0.4×10^{-12} m^{-1} s^{-1} in the eastern Atlantic (Fig. 12), which is smaller than the background Q values of 2×10^{-12} m^{-1} s^{-1} (Fig. 11).

The Q distribution over the Pacific is found to be robust to making different choices in our processing of the data, such as using a different density difference $\Delta\sigma_4$, only using the mean values of the NODC data over each of the 15° squares covering the Pacific, using the gridded climatology of Levitus et al. (1994) and Levitus and Boyer (1994a), or using a neutral surfaces definition of potential vorticity (see the appendix). Table 1 shows the correlation coefficient and the root-mean-square difference between each of these cases and our ''truth'' (Fig. 11c) with the correlation coefficient found always to be close to 1.0.

The buoyancy frequency is now shown in order to assess whether Q or N^2 appears more uniform. Here N^2 decreases poleward over almost the entire Pacific (Fig. 13). As $Q = fN^2/g$, the nearly uniform Q over the North Pacific requires this northward decrease in N^2 to compensate for the poleward increase in f. However, over

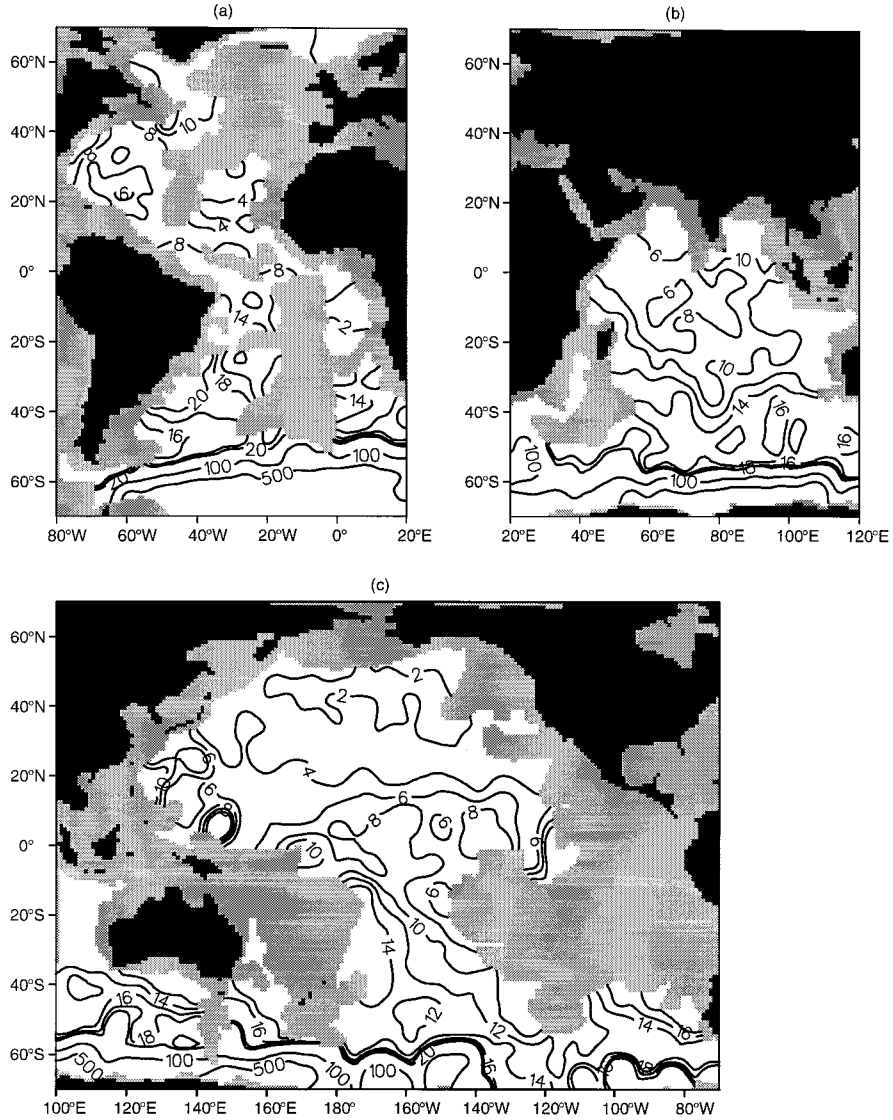

FIG. 13. Distribution of N^2 ($10^{-7}s^{-2}$) on the $\sigma_4 = 45.87$ surface in the (a) Atlantic, (b) Indian, and (c) Pacific Oceans.

TABLE 1. Comparison of different calculations of potential vorticity for the deep water with our truth in the Pacific, which uses a potential density definition with $\Delta\sigma = 0.02$ and is applied to the NODC data. The statistics are calculated from a pointwise comparison of the gridded fields north of 50°S.

Different cases	Correlation coefficient	RMS difference (10^{-12} m^{-1} s^{-1})
using $\Delta\sigma_4 = 0.04$	0.997	0.53
using $\Delta\sigma_4 = 0.01$	0.998	0.50
using mean of NODC data within 15° squares	0.984	1.25
Levitus climatology	0.974	1.61
neutral-surface PV	0.991	1.02

the eastern Atlantic, both N^2 and Q appear nearly uniform, and it is difficult to distinguish between these signals due to the small latitudinal range across the basin at this depth. In contrast, the N^2 variation appears relatively small over the western North Atlantic compared with the Q variation.

3) BOTTOM WATER: $\sigma_4 = 45.90$ SURFACE

This σ_4 surface lies at depths of typically 3.5 km in the Indian Ocean, 3.5 to 4.5 km in the western Atlantic, and 4 to 4.5 km in the Pacific Ocean, and again shoals across the ACC (Fig. 14). At these depths the Atlantic and Pacific basins have dramatically shrunk and the Indian Ocean has become subdivided.

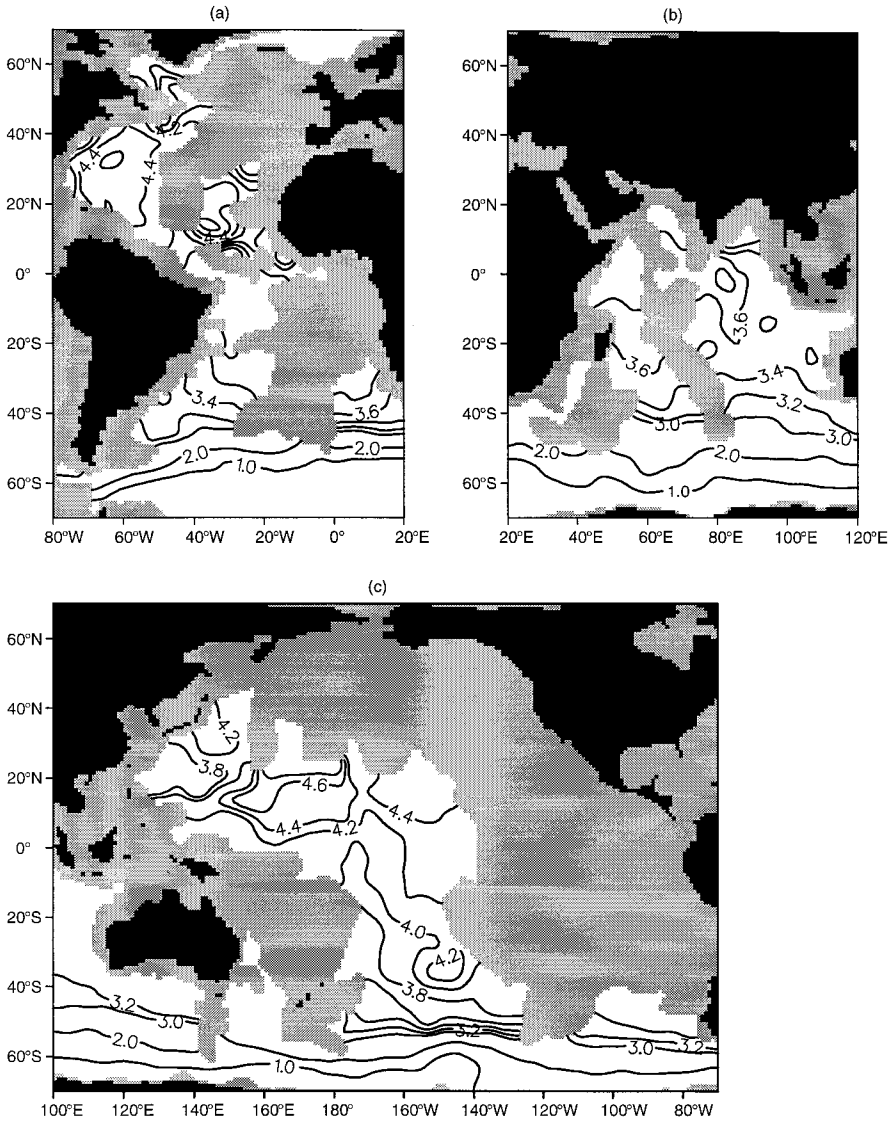

FIG. 14. As in Fig. 7 but for the depth of the $\sigma_4 = 45.90$ surface.

The Q distribution for the bottom water again reveals a rich structure (Fig. 15), which differs in detail from the patterns in the overlying deep water and is unlike the zonal distribution in the upper deep water. The western Atlantic now has a north–south asymmetry. There appears to be relatively weak and uniform Q over the northern basin, although the standard error reaches 0.6 $\times 10^{-12}$ m^{-1} s^{-1} in the interior of the basin (Fig. 16). In the southern basin, Q increases in magnitude poleward from the zero value on the equator to the high values in the ACC (where this surface is in the thermocline). However, the Q contours are now strongly inclined to latitude circles around 30°S; Q in the Indian Ocean is again generally zonal, although there are some inclined contours around 25°S.

The Q field in the South Pacific is similar to that of the deep water but with a stronger inclination of the contours away from latitude circles. In the North Pacific there is still a region of uniform Q with a value of 2×10^{-12} m^{-1} s^{-1}, but its extent has shrunk with higher values of Q appearing in the northwest corner of the basin; the standard error is still relatively small and varies typically from 0.2 to 0.4 ($\times 10^{-12}$ m^{-1} s^{-1}) in the interior of the basin (Fig. 16).

In summary, the Q diagnostics reveal regimes with Q contours following latitude circles, inclined to them, and regions of nearly uniform Q. These different regimes appear to be robust over spatial scales of several 1000 km, as the standard error is relatively small compared with these signals. However, further analysis is required to assess the temporal variability in these different regimes.

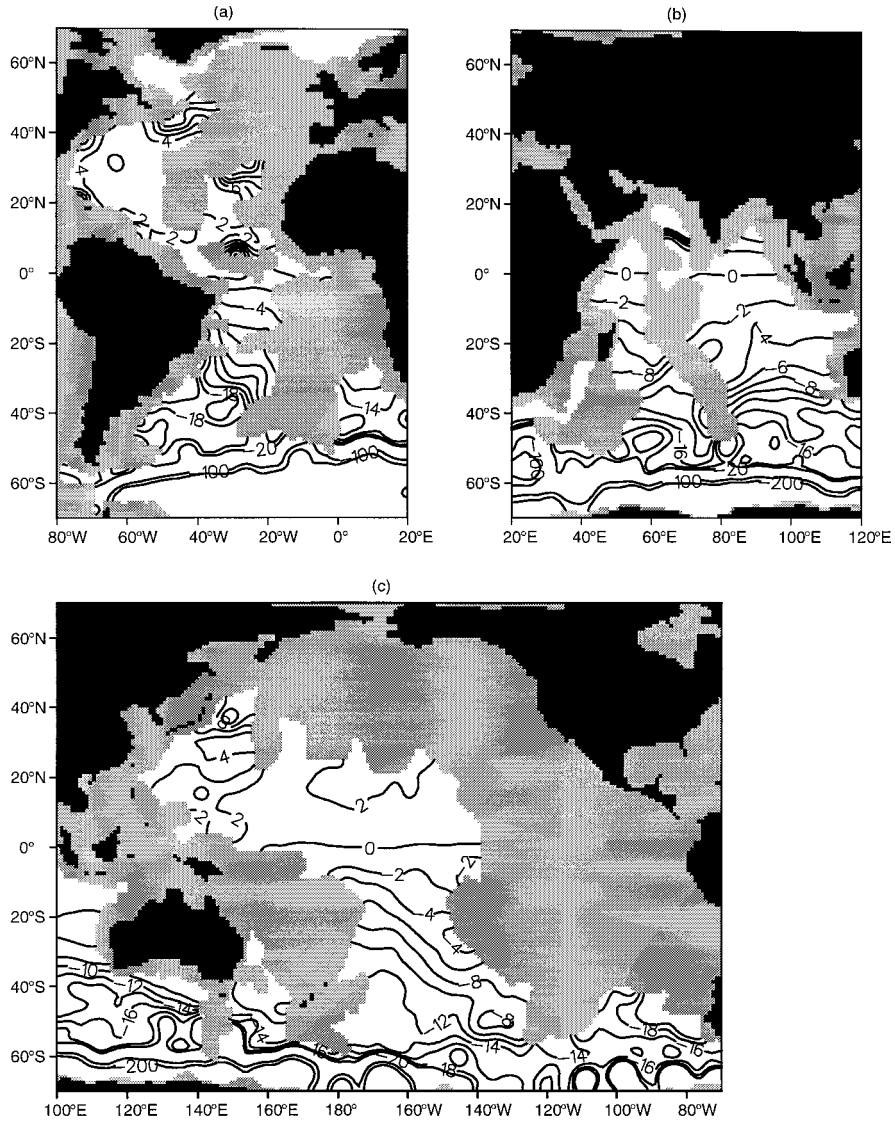

FIG. 15. As in Fig. 8 but for Q on the $\sigma_4 = 45.90$ surface with $\Delta\sigma_4 = 0.02$.

c. Speculations about the control of the Q *distributions*

The different Q distributions revealed in this climatological analysis might result from a range of mechanisms including (1) the contrast in Q values injected into a basin, (2) diabatic modification within the basin, and (3) the effect of eddy stirring.

1) The number and location of water masses ventilating a basin certainly appears to help control the Q distributions. Assuming that Q is always set to zero at the equator and that elsewhere Q is only weakly modified by forcing, then the injection of a water mass into a basin with a particular stratification will always lead to a *larger* Q contrast across the basin if the source is at high latitude than if it is at a low latitude (Fig. 17). This interpretation is supported by the nearly uniform Q having a low magnitude and occurring for the spreading of modified NADW into the North Pacific and, possibly, for the AABW into the North Atlantic and North Pacific. For the spreading of NADW into the eastern Atlantic, there may also be a physical selection by the exchange being constrained to occur through the fracture zones in the Mid-Atlantic Ridge at low latitudes. The generally zonal Q distribution for the upper deep water may reflect the lack of a strong water mass source for this layer outside the North Atlantic.
2) For water masses to spread over the globe, there clearly has to be some diabatic modification of Q. We suspect that this is achieved by enhanced mixing at special sites, rather than occurring uniformly over the interior. For example, Armi (1978) and Toole et al. (1994) observe stronger mixing near topography,

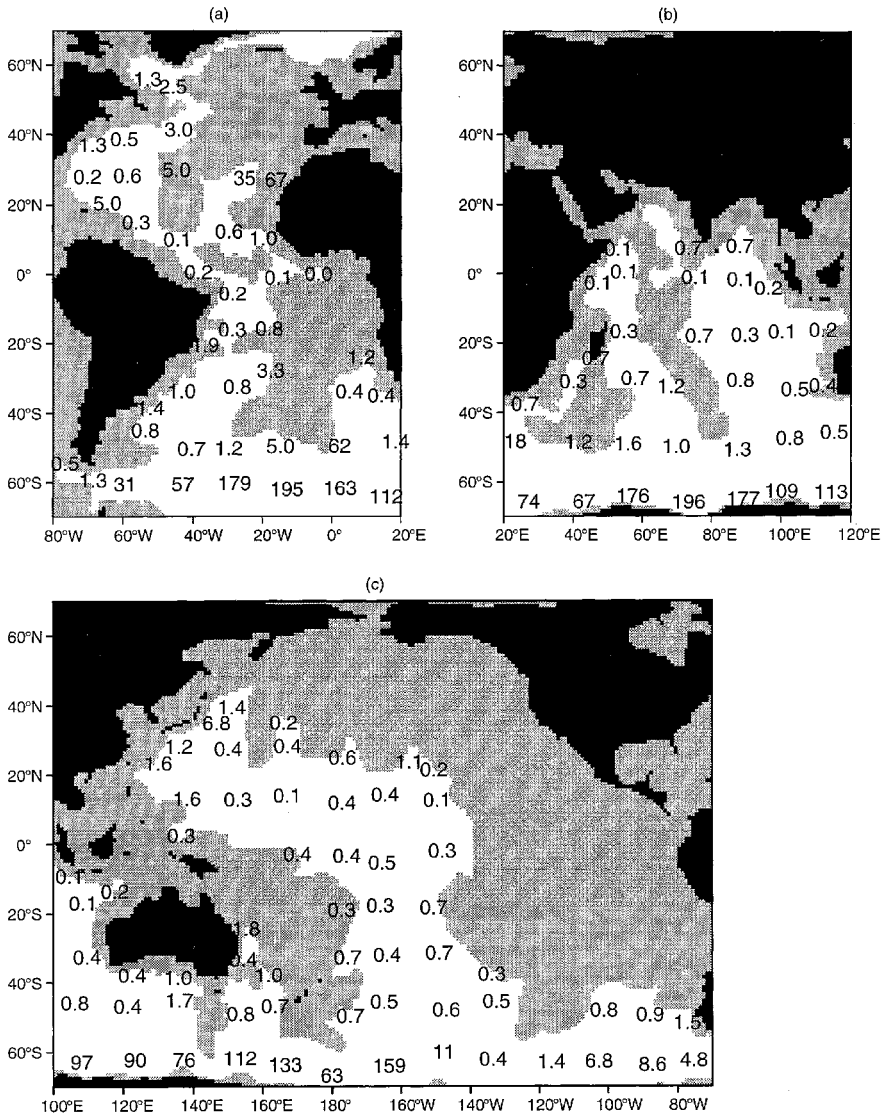

FIG. 16. As in Fig. 9 but for standard error on the $\sigma_4 = 45.90$ surface.

and Polzin et al. (1997) observe enhanced mixing for several hundred meters above rough topography, which might possibly be driven by barotropic tides interacting with topography (W. Munk and C. Wunsch 1997, personal communication). Geothermal heating may also be important in some regions of the abyssal ocean, such as the North Pacific (Talley 1988; Joyce et al. 1986). If there is inhomogeneous forcing, geostrophic streamlines should cross Q contours where there is strong forcing, but they should be coincident with each other in the unforced interior.

3) The Q distribution might reflect the long-term effect of eddy stirring tending to homogenize Q within closed geostrophic streamlines (Rhines and Young 1982a). If this a relatively weak process, then one might expect it to be masked in basins with a number of water mass sources, but instead to become apparent in relatively isolated basins. However, for this mechanism to explain the Q distribution beneath the thermocline in the North Pacific, the eddy stirring would have to be more effective at the bottom than at middepths.

To shed some light on this latter hypothesis we now diagnose the dissolved oxygen concentration for the deep water from the climatological NODC data (Levitus and Boyer 1994b) (see Fig. 18). This oxygen distribution can be interpreted in terms of the age of ventilated waters where increased age correlates with lower oxygen due to the oxidation of biological detritus. The oxygen concentration is a maximum in the western North Atlantic and off Antarctica reaching values greater than

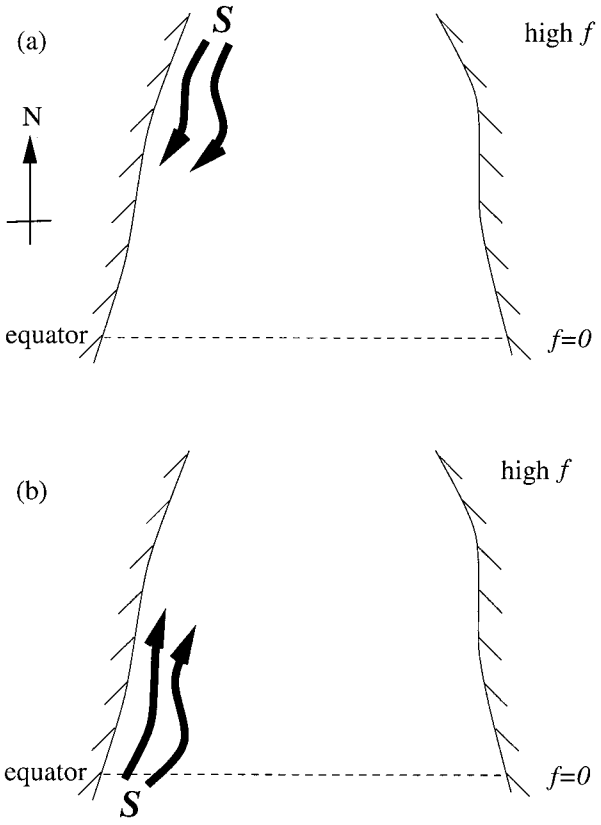

FIG. 17. A schematic figure showing a plan view of an ocean basin in the Northern Hemisphere, which has a single water mass source either (a) at northern high latitudes or (b) from the Southern Hemisphere. Assuming that Q is zero on the equator and that Q is only weakly modified in the interior, then if these different water-mass sources initially have the same stratification then there will be a larger Q contrast across the basin in (a) than in (b).

6.0 ml l^{-1}. In the Atlantic, the concentration decreases into the eastern basin. The oxygen concentration decreases further into the Indian and Pacific Ocean, reaching a minimum of 3.2 ml l^{-1} in the North Pacific. Thus, the regions of nearly uniform Q correspond with local minima in the oxygen concentration. In addition, the oxygen distribution appears relatively uniform over the North Pacific and is similar to the Q distribution there.

5. Discussion

The large-scale potential vorticity Q is diagnosed from climatology for the abyssal waters and is found to have a rich structure. There are regimes with Q contours following latitude circles, inclined to them, and even regions of nearly uniform Q. The nearly uniform Q occurs over the deep waters of the North Pacific and eastern Atlantic, and possibly the bottom waters of the western North Atlantic and North Pacific.

The different Q distributions may depend on the interplay between the different Q values injected into the basin, the recirculation timescale in the basin, and the strength of eddy mixing. A large variability in Q may be induced when there are multiple sources of deep water, each with a different characteristic value of Q. When there is a single source of Q, the resulting contrast across the basin may depend on how this source value compares with the zero value set at the equator. This view is in accord with the nearly uniform Q regions also having a *low* magnitude and occurring whenever a basin is ventilated by a single water mass entering the domain from a low latitude.

Eddy stirring tends to homogenize potential vorticity within closed geostrophic contours (Rhines and Young 1982a). For this mechanism to be relevant, the eddy activity probably has to be generated in the overlying thermocline and then transmitted down to the deep ocean. The regions of nearly uniform Q do not correspond to regions where eddy activity is expected to be large, such as near-western boundaries or the ACC, although the ratio of the eddy kinetic energy to mean kinetic energy often increases dramatically in more quiescent regions (Rhines and Schopp 1991). If eddy stirring is a relatively weak process, the homogenization is more likely to occur for poorly ventilated basins already having weak contrasts in Q. However, the eddy stirring would have to be more effective towards the bottom than at middepths in order to explain the deep Q structure in the North Pacific.

As Q is a dynamical tracer, its distribution provides some insight into possibly different dynamical regimes over the globe. While Q has to be forced and modified for any global circuit of a fluid parcel, there may be basin-scale regions over which the flow is nearly adiabatic and the Q contours are close to geostrophic streamlines. In a linear regime, Q contours follow latitude circles and any meridional flow has to be forced. However, in a more nonlinear regime, Q contours are inclined to latitude circles and any forcing might be confined to where Q contours intersect the topography—there may be a free component to the meridional flow in the interior. In the limit of nearly uniform Q, fluid parcels can freely circulate around the basin without any forcing being required at lowest order on this σ surface. However, even in these cases, the circulation is not arbitrary since the flow is connected by thermal wind to the overlying layers where there are Q gradients.

In conclusion, these Q diagnostics pose a challenge to theoretical descriptions of the deep circulation. Even though the deep circulation is weaker than that in the upper ocean, the flows are still sufficiently strong and nonlinear to modify the stratification and lead to a nonzonal Q distribution. There are even regions of nearly uniform Q in the abyssal waters when a single water mass enters a basin from low latitudes. Work is proceeding to examine whether similar patterns in Q exist within the WOCE hydrographic survey, how isolines of Q intersect streamlines, and whether this reveals any information about how the abyssal ocean is forced.

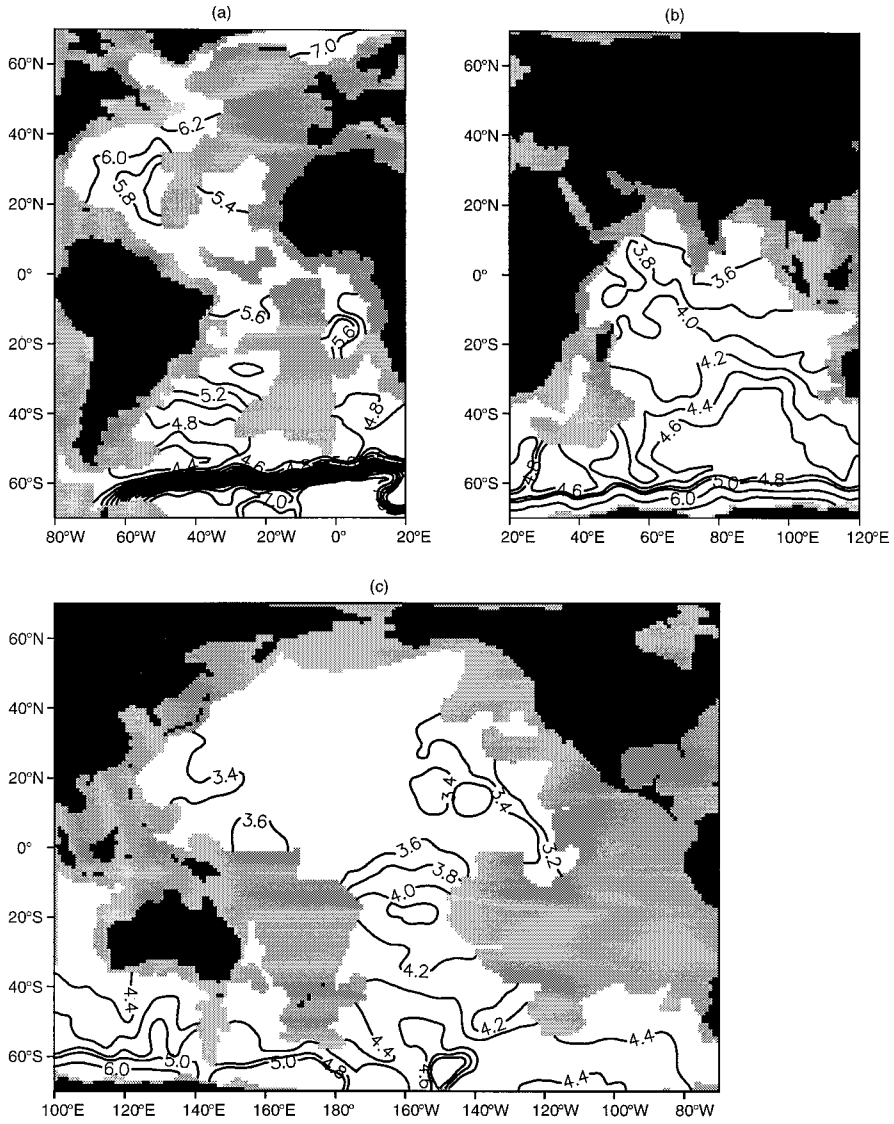

FIG. 18. Oxygen concentration (ml l^{-1}) on $\sigma_4 = 45.87$ surface in the (a) Atlantic, (b) Indian, and (c) Pacific Oceans.

Acknowledgments. The work was supported by a Ph.D. studentship GTMAS/93/WOCE/2 and a research Grant GST/02/1686 from the Natural Environment Research Council U.K. WOCE Special Topic fund. We are grateful to George Nurser for helpful discussions, and to Peter Rhines and an anonymous reviewer for useful and critical comments that led to improvements in this work.

APPENDIX

Neutral Surface Definition of Potential Vorticity

Potential vorticity may be defined in terms of the vertical spacing between neutral surfaces as advocated by McDougall (1988), rather than σ_n surfaces. You and McDougall (1990) diagnose potential vorticity from neutral surfaces (NPV) and from σ_n surfaces (Q) globally over the upper 1500 m of the ocean using climatology. They find differences between NPV and Q that can easily reach 30% in magnitude. In particular, meridional gradients in NPV and Q are found to differ over frontal zones in the thermocline. These differences are due to both the choice in the background reference pressure used for the σ_n surface and, to a lesser extent, to gradients of potential temperature along a neutral surface.

In order to assess the sensitivity of our diagnostics to our definition of potential vorticity, we calculate the NPV for a neutral surface in the deep water of the Pacific Ocean using routines from Jackett and McDougall

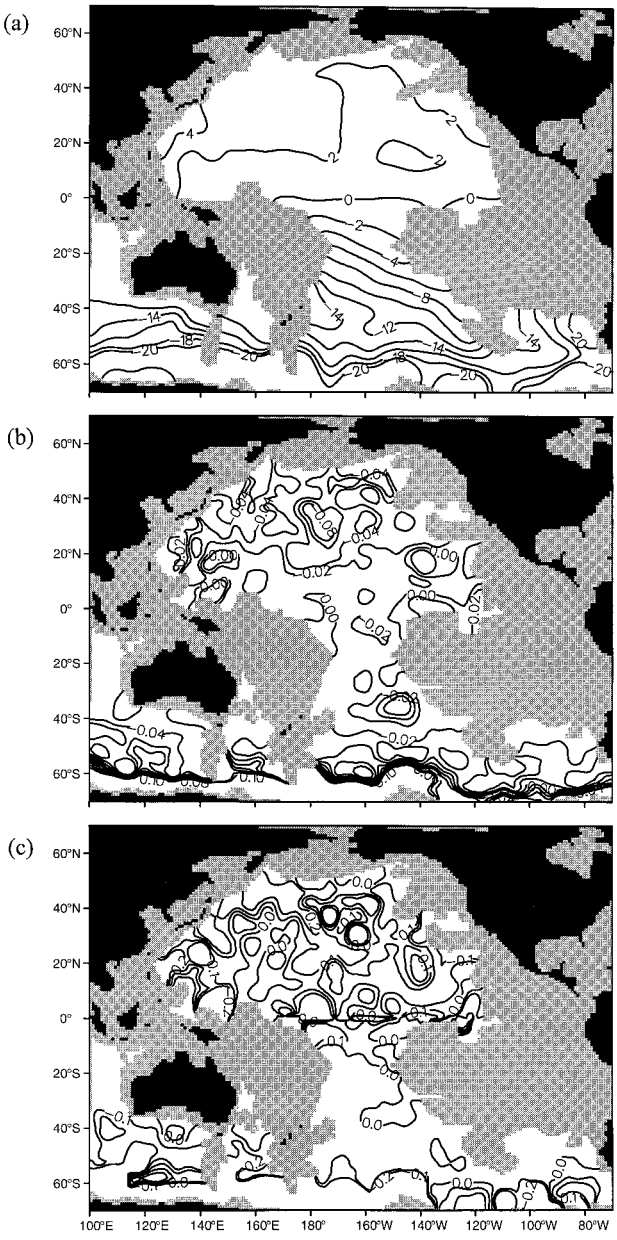

FIG. A1. Neutral surface calculations for potential vorticity and depth along the $\gamma = 28.09$ surface in the Pacific: (a) neutral-surface potential vorticity (NPV) for $\gamma = 28.09$, which should be compared with Q along the $\sigma_4 = 45.87$ surface shown in Fig. 11; (b) difference in the depths of the $\gamma = 28.09$ and $\sigma_4 = 45.87$ surfaces divided by the depth of the γ surface; (c) difference in the NPV for $\gamma = 28.09$ and Q for $\sigma_4 = 45.87$ surfaces divided by the NPV for the γ surface.

(1997). The NPV on the $\gamma = 28.09$ surface is shown in Fig. A1a, which should be compared with Q on the $\sigma_4 = 45.87$ surface shown in Fig. 11c. The patterns appear very similar with NPV contours strongly inclined to latitude circles in the South Pacific and NPV is nearly uniform in the North Pacific. The depths of the $\sigma_4 = 45.87$ and $\gamma = 28.09$ surfaces closely follow each other over most of the Pacific and only appear to deviate by more than 10% south of 55°S (Fig. A1b). The differences between Q and NPV reach 20% over small scales in the North Pacific (Fig. 19c). However, the larger-scale patterns of NPV and Q appear broadly similar. The correlation between the maps of NPV and Q is 0.991 (Table 1).

Consequently, in our study, we prefer to use the more accessible definition of potential vorticity in terms of potential density surfaces (following McDowell et al. 1982; Talley and McCartney 1982; Keffer 1985) rather than use neutral-surface potential vorticity.

REFERENCES

Armi, L., 1978: Some evidence for boundary mixing in the deep ocean. *J. Geophys. Res.*, **83** (C), 1971–1979.

Dickson, R. R., and J. Brown, 1994: The production of North Atlantic deep water: Sources, rates and pathways. *J. Geophys. Res.*, **99,** 12 319–12 341.

Hua, B. L., D. W. Moore, and S. Le Gentil, 1997: Inertial nonlinear equilibration of equatorial flows. *J. Fluid Mech.*, **331,** 345–371.

Jackett, D. R., and T. J. McDougall, 1997: A neutral density variable for the world's oceans. *J. Phys. Oceanogr.*, **27,** 237–263.

Joyce, T. M., B. A. Warren, and L. D. Talley, 1986: The geothermal heating of the abyssal subarctic Pacific Ocean. *Deep-Sea Res.*, **33,** 1003–1015.

Keffer, T., 1985: The ventilation of the world's oceans: Maps of the potential vorticity field. *J. Phys. Oceanogr.*, **15,** 509–523.

Levitus, S., and T. P. Boyer, 1994a: *Temperature.* Vol. 4, *World Ocean Atlas 1994,* U.S. Dept. of Commerce, 117 pp.

——, and ——, 1994b: *Oxygen.* Vol. 2, *World Ocean Atlas 1994,* U.S. Dept. of Commerce, 186 pp.

——, R. Burgett, and T. P. Boyer, 1994: *Salinity*. Vol. 3, *World Ocean Atlas 1994,* U.S. Dept. of Commerce, 99 pp.

Lozier, M. S., M. McCartney, and W. B. Owens, 1994: Anomalous anomalies in averaged hydrographic data. *J. Phys. Oceanogr.*, **24,** 2624–2638.

Luyten, J. R., J. Pedlosky, and H. Stommel, 1983: The ventilated thermocline. *J. Phys. Oceanogr.*, **13,** 292–309.

Mantyla, A. W., and J. L. Reid, 1983: Abyssal characteristics of the world ocean waters. *Deep-Sea Res.*, **30,** 805–833.

McCartney, M. S., 1993: Crossing of the equator by the deep western boundary current in the western Atlantic Ocean. *J. Phys. Oceanogr.*, **23,** 1953–1974.

McDougall, T. J., 1988: Neutral-surface potential vorticity. *Progress in Oceanography,* Vol. 20, Pergamon Press, 185–221.

McDowell, S., P. B. Rhines, and T. Keffer, 1982: North Atlantic potential vorticity and its relation to the general circulation. *J. Phys. Oceanogr.*, **12,** 1417–1436.

Polzin, K. L., J. M. Toole, J. R. Ledwell, and R. W. Schmitt, 1997: Spatial variability of turbulent mixing in the abyssal ocean. *Science,* **276,** 93–96.

Reid, J. L., and R. J. Lynn, 1971: On the influence of the Norwegian–Greenland and Weddell Seas upon the bottom waters of the Indian and Pacific Oceans. *Deep-Sea Res.*, **18,** 1063–1088.

Rhines, P. B., and W. R. Young, 1982a: Homogenization of potential vorticity in planetary gyres. *J. Fluid Mech.*, **122,** 347–368.

——, and ——, 1982b: A theory of the wind-driven circulation, I. Mid-ocean gyres. *J. Mar. Res.*, **40** (Suppl.), 559–596.

——, and R. Schopp, 1991: The wind-driven circulation: Quasi-geostrophic simulations for nonsymmetric winds. *J. Phys. Oceanogr.*, **21,** 1438–1469.

Schmitz, W. J., 1995: On the interbasin-scale thermohaline circulation. *Rev. Geophys.*, **33,** 151–173.

Speer, K. J., and M. S. McCartney, 1992: Bottom water flow in the western North Atlantic. *J. Phys. Oceanogr.*, **22,** 83–92.

Stommel, H., and A. B. Arons, 1960: On the abyssal circulation of the world ocean—I. Stationary planetary flow patterns on a sphere. *Deep-Sea Res.,* **6,** 140–154.

Suga, T., and L. D. Talley, 1995: Antarctic Intermediate Water circulation in the tropical and subtropical South Atlantic. *J. Geophys. Res.,* **100,** 13 441–13 453.

Talley, L. D., 1988: Potential vorticity distribution in the North Pacific. *J. Phys. Oceanogr.,* **18,** 89–106.

——, and M. S. McCartney, 1982: Distribution and circulation of Labrador Sea Water. *J. Phys. Oceanogr.,* **12,** 1189–1205.

Toole, J. M., K. L. Polzin, and R. W. Schmitt, 1994: Estimates of diapycnal mixing in the abyssal ocean. *Science,* **264,** 1120–1123.

Warren, B. A., 1981: Deep circulation of the world ocean. *Evolution of Physical Oceanography,* B. A. Warren and C. Wunsch, Eds., The MIT Press, 6–41.

Williams, R. G., 1991: The role of the mixed layer in setting the potential vorticity of the main thermocline. *J. Phys. Oceanogr.,* **21,** 1803–1814.

You, Y., and T. J. McDougall, 1990: Neutral surfaces and potential vorticity in the world's oceans. *J. Geophys. Res.,* **95,** 13 235–13 261.